

# Asymmetric aerial oxidation for applications in intracavity contacted oxide aperture VCSELs

Y. J. YOO, Y. M. SONG

*Department of Electronics Engineering, Pusan National University, Busan 609-735, Korea*

We present an asymmetric aerial oxidation that enables volume reduction and minimization of parasitic impedances in intracavity contacted vertical-cavity surface-emitting lasers (VCSELs). Thermal oxidation of AlGaAs in mesas with various geometries reveals the possibility of asymmetric aerial oxidation. Theoretical modeling results based on diffusion equation also support the experimental results. As a preliminary result, we fabricated 980 nm intracavity-contacted oxide-aperture VCSELs by using an asymmetric oxidation. The device exhibits modulation bandwidth of 11.5 GHz at a bias current of 6 mA, with a modulation current efficiency factor of 5.6 GHz/mA<sup>1/2</sup>. The proposed concept can be used for various Aluminum-oxide (AlO<sub>x</sub>)-based devices such as VCSELs, edge emitting lasers, and GaAs on insulator (GOI) field effect transistors.

(Received November 13, 2015; accepted February 10, 2016)

Keywords: Aluminum oxide, Vertical cavity surface emitting lasers, Aluminum Gallium Arsenide, Thermal oxidation

## 1. Introduction

Thermal oxidation of high aluminum content AlGaAs has received much attention due to their applications in electronic and optoelectronic devices such as edge emitting lasers, vertical-cavity surface-emitting lasers (VCSELs), and GaAs-on-insulator (GOI) field effect transistors [1-4]. For instance, VCSELs use an oxide aperture as an electrical and optical confinement layer, because aluminum-oxide (Al<sub>x</sub>O<sub>y</sub>) has electrical insulating properties, low refractive index, and good interface qualities. Furthermore, precise control of oxidation layer composition enables functional structures such as tapered oxide apertures and self-aligned microlenses [5-7]. Many studies on the modeling and experiments of thermal oxidation of AlGaAs were reported [8, 9]. By contrast, less attention has been paid to modifying the mesa geometries. To form the oxide apertures or microlenses, mesas with circular or rectangular shape is defined, because the thermal oxidation depth is isotropic in lateral direction. On the other hand, asymmetric aerial oxidation can be formed by mesa shaping with unusual geometry. These concepts could provide degree of freedom in designing device geometries for improving efficiencies or adding functionalities.

The concept of asymmetric aerial oxidation can be applied to intracavity contacted oxide aperture VCSELs, consisting of the undoped distributed Bragg reflector (DBR) mirrors and two contact layers on either side of the active region. Intracavity contacted VCSELs has many advantages such as low forward voltage, low optical loss in both undoped DBR mirrors, and coplanar contacts resulting in reduced pad capacitance [10, 11]. Moreover,

surface treatment on DBR, such as photonic crystal [12], monolithic integration of microlens [7], and high-index contrast grating [13], is favorable in intracavity structures because there are no voltage drops in undoped DBR region. However, conventional intracavity-contacted VCSELs have high lateral conduction resistance and parasitic capacitance in oxide region, degrading the modulation bandwidth. Relatively larger volume of these devices are not suitable for monolithic integration with other devices such as photodetectors [14]. The abovementioned issues can be released by incorporating the asymmetric aerial oxidation. In this paper, we introduce asymmetric aerial oxidation for applications in intracavity contacted oxide aperture VCSELs. We systematically investigate the effect of mesa geometry on the oxide aperture formation together with theoretical modeling results. With the optimized mesa geometry, we fabricate the intracavity contacted VCSELs with remarkable volume reduction, which minimize the parasitic impedances. Detailed experimental results are also discussed.

## 2. Oxidation experiments

Fig. 1 show schematic illustrations of (a) a conventional and (b) a modified intracavity-contacted oxide-aperture VCSELs. The conventional intracavity VCSELs have three circular mesas, each of which for light emitting area, p-contact, and n-contact, respectively. The overlap area between the p-doped and n-doped regions surrounding the active layers is the major contributor to the device capacitance in the conventional VCSELs. To remove a redundant area (blue color in Fig. 1(a)), we

conducted the asymmetric aerial oxidation, which means mesa shape for oxide-aperture is not a circular shape (second mesa in Fig. 1(b)). It is noted that the etching of

these unwanted area could not be a solution due to the etching difficulty of multilayer stacks including two oxidized layers.

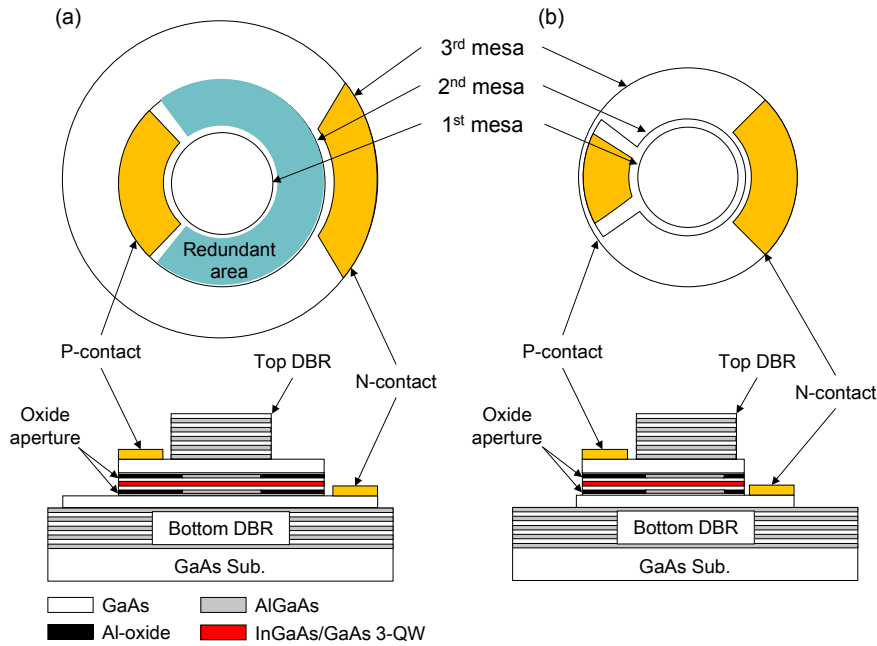


Fig. 1. Schematic illustrations of intracavity-contacted oxide-aperture VCSELs with (a) a conventional geometry and (b) a proposed geometry incorporating asymmetric aerial oxidation.

To investigate the validity of an asymmetric aerial oxidation, we grew an epitaxial layer structure, as shown in Fig. 2(a). A 100-nm GaAs buffer layer was grown on the epi-ready GaAs substrate followed by 50-nm  $\text{Al}_{0.98}\text{Ga}_{0.02}\text{As}$  oxidation layer. The structure was then capped with a 100-nm GaAs layer. After the growth of the epitaxial layer, standard photolithography was used to pattern modified mesas, which are similar with second mesa of Fig. 1(b). The GaAs cap and AlGaAs layers were etched by  $\text{SiCl}_4\text{-Ar}$  plasma in an inductively coupled-plasma (ICP) etching system for lateral oxidation. The etched samples were oxidized at a temperature of  $400^\circ\text{C}$  for 25min (See Fig. 2(b)). Water vapor atmosphere was created by bubbling  $\text{N}_2$  carrier gas at 2 l/min through water bubbler maintained at  $90^\circ\text{C}$ . During the oxidation process, reaction of the oxidant with AlGaAs transforms the AlGaAs into oxide, meanwhile, oxidation by-products  $\text{AsH}_3$  and  $\text{H}_2$  diffuse out. More detailed oxidation kinetics can be found in other literature [7, 8]. Fig. 2(c) and (d) shows microscopic top view image of asymmetric mesas (c) before and (d) after thermal oxidation. The oxide aperture diameter was  $\sim 8\ \mu\text{m}$  and an oxidation profile exhibits a circular shape, which are applicable to the modified intracavity contacted VCSEL structures. This oxidation process also yields very high repeatability.

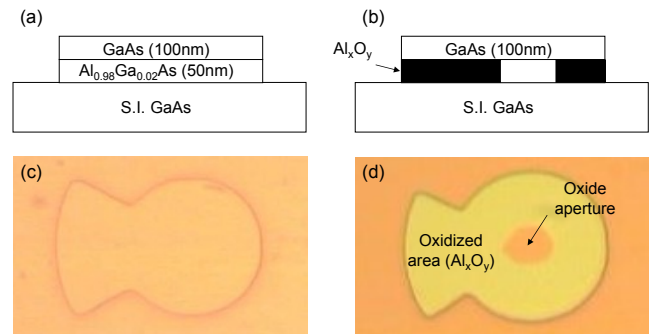


Fig. 2. (a, b) Epitaxial layer structure for experiments of asymmetric aerial oxidation ((a) before and (b) after oxidation), (c, d) Microscopic top view of modified mesa (c) before and (d) after oxidation.

Fig. 3 shows detailed experimental results on the asymmetric aerial oxidation. We conducted the thermal oxidation for mesas with different geometries. As expected, the mesas with combined circle/sector shapes provide asymmetric oxidation areas. As the sector angle decreases from  $135^\circ$  to  $60^\circ$ , the oxide aperture transforms to circular shape, which is almost same as the shape formed by circular mesa (Fig. 3(f)). On the other hand, smaller sector angle allows only limited spaces for metal contacts, which lead increased ohmic resistance, especially in p-GaAs areas. This adverse effect can be relaxed by using a stitched sector geometry, as shown in Fig. 3(d) and (e). Stitching of sector area induces uniform oxidation in the circular region, resulting a circular oxide aperture as well

as increased contact area. It is also noted that larger gap between sectors provide more uniform oxide aperture, as indicated in Fig. 3(e).

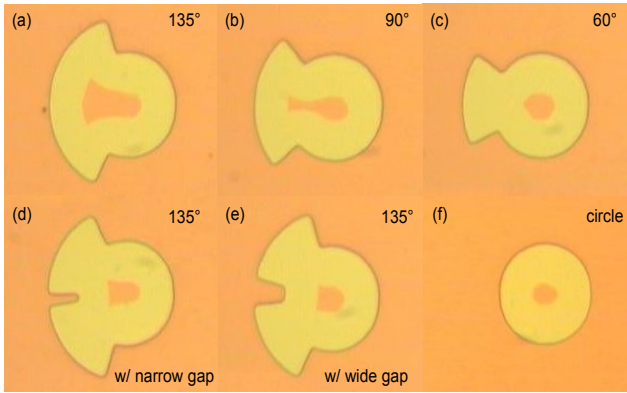


Fig. 3. Microscope images of six different mesas after thermal oxidation (i.e., (a-c) circle-sector geometry with a sector angle of (a) 135°, (b) 90°, and (c) 60°, respectively, and (d, e) stitched sector geometry with (d) a narrow gap and (e) a wide gap, and (f) conventional circular shape).

The oxidized area of AlGaAs can be estimated by simple modeling based on diffusion equation. Because of the conservation of oxidant mass, the oxidant transport through the material is governed by the equation as follows:

$$\frac{\partial \rho(x)}{\partial t} = \nabla \cdot (D \nabla \rho(x)) - v(x) \rho(x)$$

Where  $\rho(x)$  and  $v(x)$  is concentration and velocity of the oxidant at position  $x$ , respectively.  $D$  is the diffusion coefficient. In this calculation, we used a commercial software (COMSOL Multiphysics, USA) with parameters obtained from literatures [8, 9]. We assumed that the temperature is uniform throughout the sample. Fig. 4 shows the calculation results of oxidation with same geometries depicted in Fig. 3. The modeling results are strongly matched to the experimental results. Some loss of edge sharpness is attributed from the parameter mismatches between modeling and experiment. Since other parameters, such as initial mesa size, oxidation temperature, and aluminum composition, affect to the shape of oxidized area, further optimization should be conducted by considering the device fabrication details.

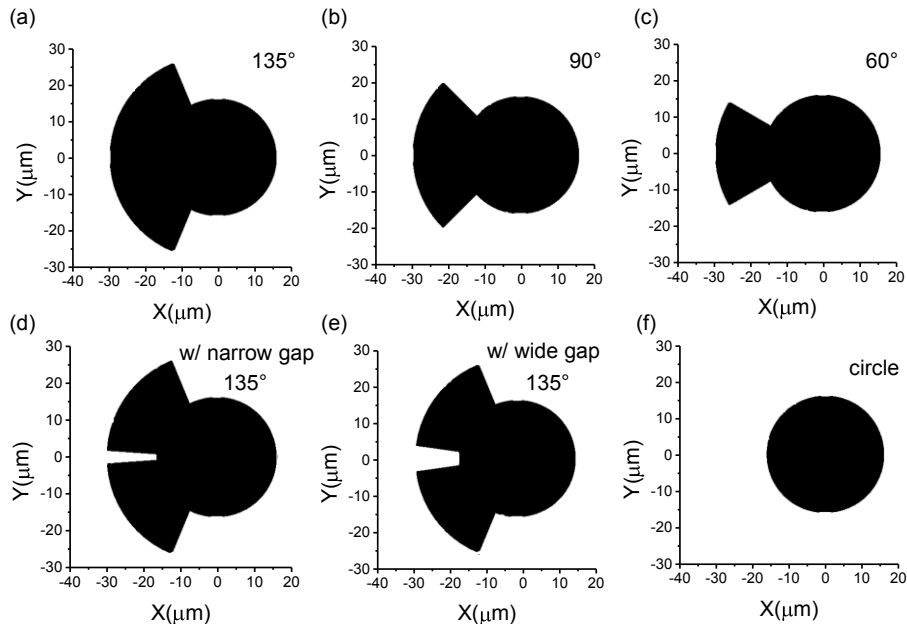


Fig. 4. Simulated two-dimensional oxidation results based on diffusion equation for six different mesas shown in Fig. 3.

### 3. Fabrication and results

After confirmation of the validity of asymmetric oxidation, as a preliminary result, this technique was employed in the fabrication of modified intracavity-contacted oxide-aperture VCSELs. All epitaxial layers were grown on semi-insulating GaAs substrate using a molecular beam epitaxy system (DCA P600). The top and bottom DBR mirrors consists of 22 and 30.5 pairs of undoped GaAs/Al<sub>0.88</sub>GaAs layers, respectively. The active region consists of 1λ cavity with three In<sub>0.19</sub>GaAs/GaAs

(8.5/10 nm) quantum wells surrounded by Al<sub>0.3</sub>GaAs cladding layers. The cavity is bounded on each side by Al<sub>0.98</sub>GaAs oxidation layers, followed by p- and n-doped GaAs contact layers. The thickness of contact layers was used 5/4λ thick in order to suppress the current crowding effect and to reduce the series resistance [11].

Device fabrication began with the formation of cylindrical mesa (first mesa) of 20 μm in diameter etched down to the p-GaAs contact layer using inductively coupled plasma etcher. Next, second mesa, having a modified shape (i.e., stitched sector geometry), was etched

down to n-GaAs contact layer. For electrical and optical confinement, two AlGaAs layers were selectively oxidized by wet thermal oxidation process. After n-contact layer was etched for device isolation, Benzocyclobutene (BCB) was coated on the sample and cured at 210°C for 1 hour for passivation and planarization. After exposing the p- and n-GaAs contact layers, Pt/Ti/Pt/Au and Ni/Au/Ge/Ni/Au were deposited on the p- and n-GaAs contact layers, respectively. The p- and n-contacts were shaped to the opposite side to reduce the current crowding at the perimeter of the oxide aperture. Contacts were alloyed for 25 seconds at 425°C.

Fig. 5 shows the light-current-voltage (LIV) characteristics of the fabricated VCSELs with 6  $\mu\text{m}$  oxide aperture diameter measured using an Agilent 4156C semiconductor parameter analyzer and a silicon photodiode with an active diameter of 10 mm. The device exhibits a low threshold current of 0.6 mA and a slope efficiency of 0.23 mW/mA. The series resistance is approximately 198  $\Omega$ , which is smaller than that of conventional intracavity VCSELs due to reduced device area. It is remarkable that the total area for intracavity VCSELs is strongly reduced from  $1936\pi\mu\text{m}^2$  to  $729\pi\mu\text{m}^2$ , which is attributable to small form factor and reduced impedance. The maximum output power is 1.18 mW at room temperature and the rollover current is around 8 mA. The small-signal modulation response was measured using a 30 GHz RF spectrum analyzer with 25 GHz high-speed photodetector. 40 GHz bias tee was used to combine DC bias and RF signal from 20 GHz continuous wave generator. Fig. 6 shows a small signal modulation response of the VCSEL with 6  $\mu\text{m}$  oxide aperture under different bias currents at room temperature. The maximum 3dB bandwidth of 11.5 GHz was obtained at a bias current of 6 mA. The modulation current efficiency factor (MCEF), meaning a linear interrelationship between the 3dB bandwidth and the square root of the driving current above threshold, was approximately  $5.6\text{ GHz}/\text{mA}^{1/2}$ .

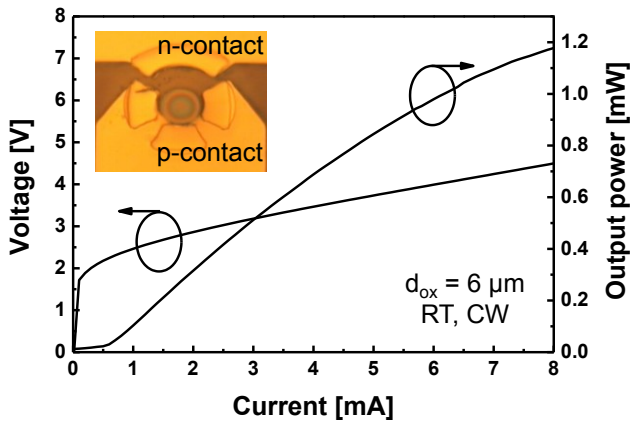


Fig. 5. Light-current-voltage curves of the fabricated VCSELs with an oxide aperture of 6  $\mu\text{m}$ .

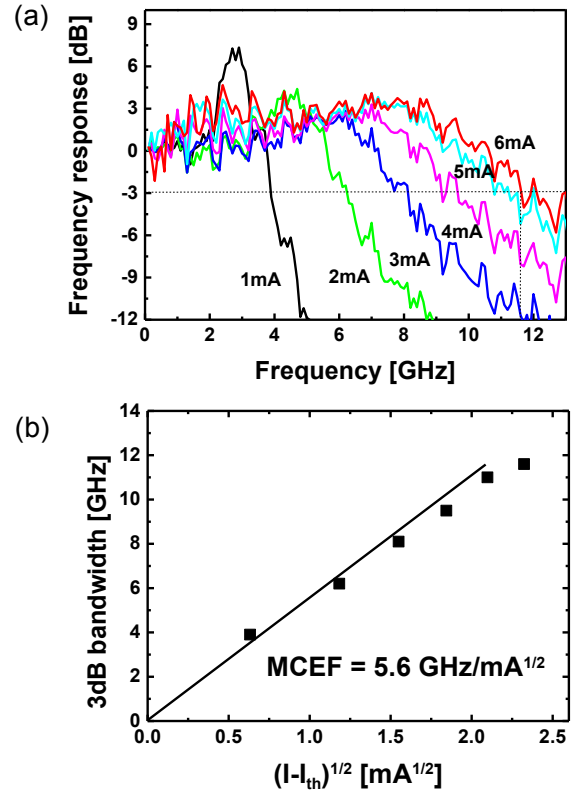


Fig. 6. (a) Small-signal modulation response of the VCSEL at various bias currents and (b) 3dB frequency bandwidth versus square root of the current above threshold.

#### 4. Conclusion

We presented the asymmetric aerial oxidation method for improving the performance of intracavity contacted oxide-aperture VCSELs. We showed that the asymmetric aerial oxidation provide circular oxide apertures while minimizing device area. After oxidation experiments with modeling, high speed operation of intracavity-contacted oxide-aperture VCSELs with asymmetric aerial oxidation was also presented. The devices exhibited a 3 dB bandwidth of 11.5 GHz and an MCEF of  $5.6\text{ GHz}/\text{mA}^{1/2}$ , making these devices suitable for high-speed optical interconnects. Further improvements of device characteristics can be substantially realized by geometry optimization. It is believed that the proposed concept can be used for various  $\text{Al}_x\text{O}_y$ -based devices such as VCSELs, edge emitting lasers, and GaAs on insulator (GOI) field effect transistors.

#### Acknowledgements

This work was partly supported by Basic Science Research Program through the National Research Foundation of Korea (NRF) funded by the Ministry of Science, ICT & Future Planning (2014R1A1A1005945), and by the National Research Foundation of Korea (NRF) Grant funded by the Korean Government (MSIP) (No.2015R1A5A7036513).

**References**

- [1] S. Y. Tzeng, M. J. Cich, R. Zhao, H. Feick, E. R. Weber, *Appl. Phys. Lett.* **82** (2003) 1063.
- [2] T. J. Jenkins, L. Kehias, P. Parikh, J. Ibbetson, U. Mishra, D. Doctor, M. Le, J. Pust, D. Widman, *IEEE J. Sol.-Stat. Circuits* **34** (1999) 1239.
- [3] S. P. Nabanja, L. A. Kolodziejski, G. S. Petrich, M. Y. Sander, J. L. Morse, K. Shtyrkova, E. P. Ippen, F. X. Kärtner, *J. Appl. Phys.* **113**, 163102 (2013).
- [4] Y.-C. Chang, L. A. Coldren, *Appl. Phys. A* **95**, 1033 (2009).
- [5] M. J. Noble, P. Sotirelis, J. A. Lott, J. P. Loehr, *SPIE* **3944**, 252 (2000).
- [6] K. S. Chang, Y. M. Song, Y. T. Lee, *IEEE Photon. Technol. Lett.* **18**, 121 (2006).
- [7] K. S. Chang, Y. M. Song, Y. T. Lee, *IEEE Photon. Technol. Lett.* **18**, 2203 (2006).
- [8] P.-C. Ku, C. J. Chang-Hasnain, *IEEE J. Quant. Electron.* **39**, 577 (2003).
- [9] J. M. Dallesasse, N. Holonyak Jr., *J. Appl. Phys.* **113**, 051101 (2013).
- [10] J. W. Scott, B. J. Thibeault, D. B. Young, L. A. Coldren, F. H. Peters, *IEEE Photon. Technol. Lett.* **6**, 678 (1994).
- [11] A. V. Krishnomoorthy, L. M. F. Chirovsky, W. S. Hobson, J. Lopata, J. Shah, R. Rozier, J. E. Cunningham, L. A. D'Asaro, *IEEE Photon. Technol. Lett.* **12**, 609 (2000).
- [12] P. O. Leisher, A. J. Danner, K. D. Choquette, *IEEE Photon. Technol. Lett.* **18**, 2156 (2006).
- [13] I. S. Chung, J. Mork, P. Gilet, A. Chelnokov, *IEEE Photon. Technol. Lett.* **20**, 105 (2008).
- [14] Y. M. Song, G. W. Ju, H. J. Choi, Y. W. Lee, B. H. Na, Y. T. Lee, *Electron. Lett.* **51**, 782 (2015).

---

\*Corresponding author: ymsong81@gmail.com